SUB-THz EM CHARACTERIZATION OF COATED MATERIALS

A. Passarelli†, H. Bartosik, G. Rumolo, CERN, 1211 Geneva 24, Switzerland
V. G. Vaccaro, M. R. Masullo, C. Koral, INFN Naples Unit, 80126 Napoli, Italy
A. Andreone, Physics Department, University of Naples Federico II, 80126 Napoli, Italy
O. Boine-Frankenheim, T.U. Darmstadt, Schlossgartenstrasse 8, 64289 Darmstadt, Germany

Abstract

The electromagnetic characterization of coating materials is fundamental to build a reliable impedance model of any accelerator. In particular, since the CLIC (Compact LInear Collider) necessitates bunches with short longitudinal length, a full electromagnetic characterization of the coating material surface impedance is needed at high frequencies in the millimetric wave length and beyond. The goal of this paper is to develop a measurement method to characterize the coating materials in the sub-THz frequency range. The electromagnetic characterization of the material is performed using a time domain coherent THz spectrometer. The method is based on the attenuation measurement of the signal passing through a waveguide specifically designed, having a very thin central layer where the coating material is deposited on both sides. The guide is equipped with two "horn" antennas integrated on both sides of the device to enhance the electromagnetic signal collection. This novel technique is tested on slabs coated with a Non-Evaporable Getter (NEG) and allows evaluating the surface impedance in the frequency range from 0.1 to 0.3 THz.

INTRODUCTION

The main goal of this paper is to develop a measurement method for the electromagnetic characterization of the coating material used in accelerator beam pipes. The coating materials requiring a characterization of their surface impedance are the amorphous Carbon (a-C), used for electron cloud mitigation [1] and the Non-Evaporated Getter (NEG), used to reach the ultra-high vacuum condition in the accelerator chambers [2]. The electron cloud in positron rings is a mechanism that starts when the synchrotron radiation photons, emitted by the beam, create a large number of photo-electrons at the inner chamber wall surface. These primary electrons, after being accelerated in the electric field of a passing bunch, may again hit the inner wall of the beam pipe, causing secondary emission or being elastically reflected [3]. If the secondary electron yield (SEY) of the surface material is greater than unity, the number of electrons grows exponentially leading to dynamic instabilities and many other side effects [4, 5].

In order to lower the value of SEY of the pipe walls, a-C coatings have been extensively tested [1] and used [6] at the CERN SPS accelerator and in other experiments [7] with very effective results.

The Ultra-High Vacuum is needed in particle accelerators to reduce the gas-beam scattering, the risk of high voltage discharge and to improve the thermal insulation [8]. The application of NEG coatings allows a distributed and continuous pumping in large accelerator vacuum chambers even in very narrow beam pipes. CERN was the pioneer in NEG thin film coating technology [9], these coatings are currently used in the LHC warm vacuum pipes. Furthermore, other accelerators like ESRF, ELETTRA, SOLEIL, MAX IV and Sirius widely employ NEG pumps in their chambers.

These coatings used for the reduction of SEY or for the improvement of the pumping processes, change the vacuum chamber surface impedance. A reliable impedance model, including a resistive wall contribution, requires an accurate electromagnetic characterization of these materials [10].

Among the NEG alloys, the alloy made from titanium (Ti), zirconium (Zr) and vanadium (V) has the lowest activation temperature at 180 degrees [11]. The surface impedance of samples coated with this NEG alloy has been evaluated for our study. We decided to test our methodology with NEG deposition whose production, with the desired thickness of 5μm, is simpler compared to a-C. Therefore, the investigation on the a-C has been postponed. As described above, there is the need to create a reliable system for measuring the surface impedance of the materials used on the coating sample. The NEG characterization of different samples has already been carried out in another paper [12, 13] by comparing numerical simulations and experimental measurements in the sub-THz frequency range.

The methodology presented in this work was studied with the idea of overcoming some of the inconveniences of the method reported in [12]:

- non-homogeneous deposition with unpredictable thickness and relevant peel-off and blistering;
- the impossibility to reuse the system for further measurements.

It has to be underlined that the NEG properties vary with the parameters of the specific coating process, like pressure in the vacuum chamber and/or voltage applied to the cathode. This means that any measurement will be not valid for NEG in general but relevant to the coating process.

This work is the first step to develop a reliable, manageable and inexpensive system for measuring the surface impedance in the sub-THz region.

METHOD

As mentioned above, the resistive wall impedance is an essential contributor for a detailed machine impedance model. In this evaluation, the EM characterization of the vacuum chamber coatings up to high frequencies may be

crucial as for CLIC DRs because of their 1.8 mm rms bunch length [14].

The goal of this work is to develop a new method to give a reliable estimation of the surface impedance of the coated material as a function of frequency. This method proposes to measure the attenuation of the signal passing through a waveguide (see Fig.1) with coated material placed on a copper foil interposed between the two shells of the waveguide. The conductivity value of the material is estimated by inspecting and comparing the theoretical and measured behavior of the attenuation due to the presence of the coating. From that value and from the measured coating thickness we may infer the surface impedance.

The waveguide is placed in the optical path of a time-resolved coherent THz spectrometer, described in detail in the next subsection.

The evaluation of the signal attenuation due to the presence of the sample allows to retrieve the conductivity by using a reference signal passing through the waveguide with copper slab without coating.

The analytical evaluation has been performed by studying the mode propagation in the Device Under Test (DUT). The analytical results are compared with Frequency domain CST simulations [15]. In the second subsection, we show the waveguide used for the experiment and the longitudinal cut where the foil is placed. To avoid coating inhomogeneity, the thickness cannot be bigger than 5-6 μm.

The measurement setup

Tera K15 of the Menlo Systems is the device used for measurements. It is a Time Domain THz spectrometer. The opto-mechanical setup used for our experiment is shown in Fig. 1.
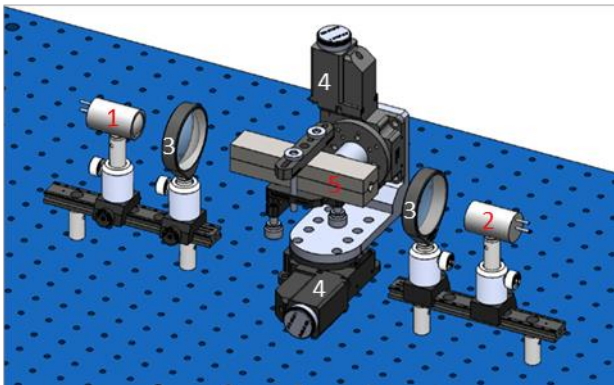

Figure 1: Sketch of the opto-mechanical setup utilized for the measurements: 1)Emitter, 2)Detector, 3)TPX collimating lenses, 4)Micrometric alignment systems, 5)DUT.

The system is based on a 1064 nm fiber laser with 120 fs pulse width and 60 MHz repetition rate. In the standard setup, the laser output splits in 2 beams.

The pump beam generates an electromagnetic transient (THz pulse, $\approx$ ps) through the excitation of a low-temperature grown GaAs based photoconductive antenna (PCA) emitter, whereas the probe beam is used to detect

the THz pulse using a similar PCA receiver. A mechanical optical line (Delay Line) is used to control the delay between probe and pump beams.

This method of detection provides the waveform, that is the electric field amplitude of the THz pulse as a function of the timing difference (see the nominal time domain signal in Fig. 2). For our evaluation, the signal is then converted into the frequency domain using a standard Discrete Fourier Transform (DFT). In the experiment, the maximum frequency resolution is about 4 GHz, limited by the scanning range of the delay line only.
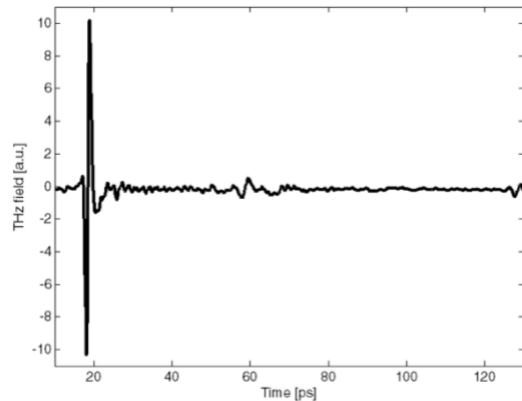

Figure 2: THz time domain signal propagation in free space.

The device under test

The device used for our experiment is shown in Fig. 3. It is a circular waveguide connected to two pyramidal horn antennas on both sides in order to enhance the electromagnetic signal collection and radiation [16]. Likely, this shape has been chosen because it is easier to mill a pyramidal horn than to machine a conical one. Conversely, to drill a cylindrical waveguide is easier to mill a rectangular one.
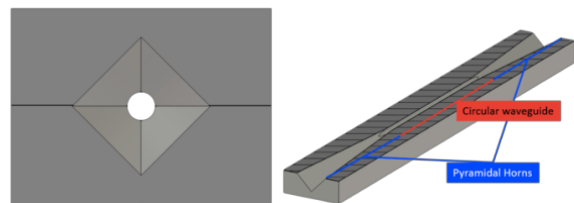

Figure 3: Circular waveguide with two pyramidal horns. Left: Front view. Right: Perspective view of longitudinal cut.

Furthermore, the transition from the horn to the waveguide is smoother than the one obtainable in case of waveguides with a conical-cylindrical or pyramidal-square transition. This can be understood by looking at the magnified stretch of transition in Fig. 4
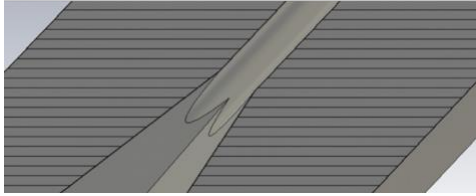
Figure 4: Magnification of the transition between the pyramidal horns and the cylindrical waveguide.

The transition curves are branches of very flat ellipses, which are the intersection between a plane and a circular cylinder. They are very flat since the plane is almost parallel to the axes of the ellipses. Therefore, this behavior smoothes the transition from the pyramidal mode to the cylindrical one. In the analytical evaluation, without affecting the results [17], we assume an abrupt transition where the pyramidal horn stops and the cylindrical waveguide starts at a plane orthogonal to the axis. The distance of this plane from the apexes of the ellipses is the double of the one to the cusp made by two ellipses. The external shape of the device under test is a parallelepiped of size *16×12×120* mm. The internal dimensions are reported in table I.

The slab has the same length as the DUT and is 50 μm thick. During the deposition process, in order to prevent the deformation, the slab is held in an aluminum frame (see Fig. 5).

Table 1: Waveguide internal dimensions.

[mm]	Length	Radius/Side (ext→int)
Cylindrical waveguide	42	0.9
Pyramidal horn	39	6→1.2728

Figure 5: Slab placed in the frame for the deposition.

The TE-VSC-SCC section at CERN performed the deposition process on both sides of two different copper slabs by using a DC magnetron sputtering technique. X-ray fluorescence (XRF) test were performed along the median line of the slab to check the thickness of the coating deposition (see Fig. 6). The slab has been placed between the two shells in such a way that the median line of the slab coincides with the center of the waveguide.
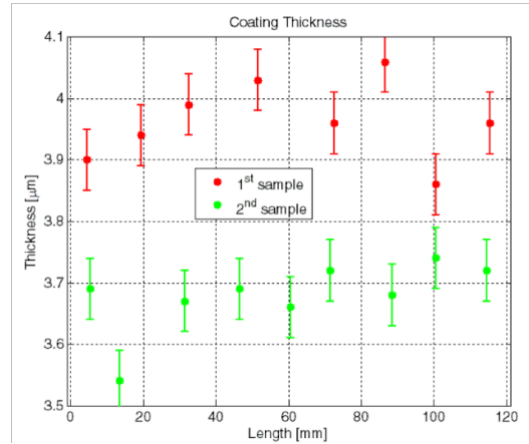

Figure 6: NEG coating deposition thickness on two slabs used for the experiments.

Modes propagating in the waveguide

In order to simplify the analysis, we decided to work with a single mode propagating in the waveguide. The first mode $TE_{1,1}$ propagating inside the circular waveguide is shown in Fig. 7 [18].

The presence of a slab placed in the median plane together with the incident wave conformation (quasi-plane wave) select the modes that can propagate inside the waveguide. The electric field must be orthogonal and continuous (above-below) to the slab surface. Furthermore, some symmetries have to be satisfied (left-right). The above sentence can be condensed in the statement: the projection of the incident plane wave on the mode must be non-null. The second mode that is allowed to propagate is the $TE_{1,2}$, all the other modes in between cannot propagate. Therefore, the allowed bandwidth is defined by the cut-off frequencies of $f_{TE1,1}$ = 97.6 GHz and $f_{TE1,2}$ = 282.6GHz. In sum, we may work in a bandwidth of about 200 GHz.
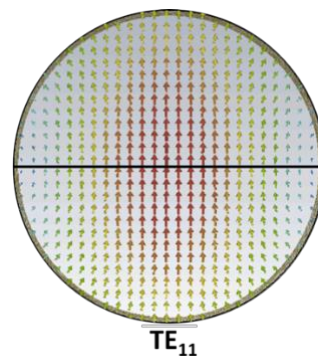

Figure 7: First mode propagating inside the cylindrical waveguide with a foil placed on the center.

Since the semi-aperture of the pyramidal horn is < 5 deg we may consider the modes which propagate in a locally uniform square waveguide and take the relevant lower modes. The first two modes, having the same cut-off frequency, are two degenerate modes. If their excitation coefficient has the same amplitude, their sum will exhibit an electric field everywhere orthogonal to the horizontal diagonal as shown in Fig. 8
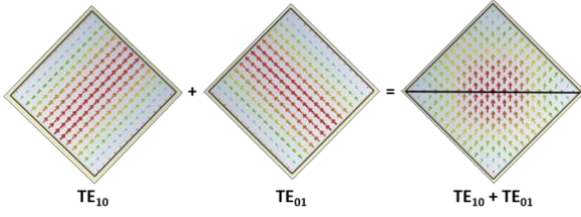
Figure 8: Electric field of the first two degenerate modes inside the square waveguide and sum (right) of the first two modes propagating inside the waveguide with a foil placed on the center.

Doing the same considerations we did for the cylindrical waveguide and considering a waveguide of side of 1.2728 mm, the sum of the first two modes allowed to pass have a cut off frequency of $f_{TE1,0} = f_{TE0,1} = 117.8$ GHz. The other two modes allowed to pass start their propagation from $f_{TE2,1} = f_{TE1,2} = 263.3$ GHz.

Considering negligible the attenuation contribution given by the transitions between the pyramidal horns and the central cylindrical waveguide, the frequency range goes from 118 GHz to 283 GHz.

THE ATTENUATION

We look for a simple and flexible tool able to yield numerical values of the signal attenuation occurring in the waveguide with the slab.

General formulation

In this section we give the general definition of attenuation in a waveguide and we evaluate it in the specific case of the waveguide used for measurements.
The definition of the attenuation constant is expressed by the formula [19, 20]:

$$\alpha = -\frac{1}{2P(z)}\frac{dP}{dz} \qquad (1)$$

where P is the total power flow at z and -dP is the power dissipated in a section of waveguide of length dz.
From Eq. 1 follows that the attenuation constant due to losses on guide walls is [19]:

$$\alpha = \frac{1}{2}\frac{Re[Z_S(z)]}{Re[Z(z)]}\frac{\int |H_{tan}|^2 ds}{\iint |H_t|^2 dS} \qquad (2)$$

where Z_S is the equivalent surface impedance, Z is the characteristic impedance of the propagating mode and H_{tan} and H_t are the nondissipative values of the magnetic field tangential to the guide periphery and transverse to the guide cross section, respectively. The line integral with respect to ds extends over the guide periphery, and the surface integral with respect to dS extends over the guide cross section. We consider the propagation of the sole $TE_{1,1}$ mode in the cylindrical waveguide. The attenuation of this single mode in a generic waveguide is:

$$A_{cyl} = \frac{1}{2}\frac{Re(Z_S)}{Re(Z_{1,1})}\frac{\int_l |n \times H_{1,1}|^2 dl}{|I_{1,1}|^2} \qquad (3)$$

where $Z_{i,j}$ is the i,j mode impedance and $I_{i,j}$ is the relevant excitation current. To evaluate the attenuation in the pyramidal transition we consider the sum of two modes, the formula in this case is:

$$A_{pyr} = \frac{1}{2}Re(Z_S)\frac{\int_l |n \times (H_{1,0}+H_{0,1})|^2 dl}{Re(Z_{1,0})|I_{1,0}|^2+Re(Z_{0,1})|I_{0,1}|^2} \qquad (4)$$

Z_S of the formulas 3 and 4, in case of coating, is:

$$Z_S = Z_{coat}\frac{Z_{cu}+jZ_{coat}tan(k_{NEG}d)}{Z_{coat}+jZ_{cu}tan(k_{NEG}d)} \qquad (5)$$

where d is the coating thickness. When d = 0 there is no coating and $Z_S = Z_{cu}$.
The characteristic impedance in the Leontovich approximation for a metallic case ($\varepsilon'' \gg \varepsilon'$) is [17]:

$$Z = (1+j)\sqrt{\frac{\omega\mu}{2\sigma}} = \frac{1+j}{\sigma\delta} \qquad (6)$$

and the propagation constant in the same condition is:

$$k = (1-j)\sqrt{\frac{\sigma\omega\mu}{2}} = \frac{1-j}{\delta} \qquad (7)$$

where δ is the skin-depth defined as:

$$\delta = \sqrt{\frac{2}{\sigma\omega\mu}} \qquad (8)$$

and $\mu = \mu_r\mu_0$ is the total permeability, μ_r the relative magnetic permeability, μ_0 the permeability of free space, $\omega = 2\pi f$ and σ the material conductivity.
As stated in the introduction, the procedure consists in the measurement and/or in the analytical evaluation of the relative attenuation defined as:

$$RA \triangleq A^{coat} - A^{cu} \qquad (9)$$

This means that the attenuation on the wall is simplified in the above formula and we have to analytically evaluate only the attenuation on the slabs.

Estimation on the foil in the cylindrical waveguide

The first mode in the cylindrical waveguide with a foil placed in the center is shown in Fig. 7.
The constant of attenuation on the foil placed in the center of a cylindrical waveguide is:

$$\alpha_{\mathrm{cyl}} = 4Re(Z_S) \frac{\chi'_{1,1} k_{z_{1,1}}}{\pi a_0 Z_0 k_0 (\chi'^2_{1,1} - 1) J_1^2(\chi'_{1,1})}$$

$$\left[\frac{k_{t_{1,1}}^2}{k_{z_{1,1}}^2} \oint_0^{\chi'_{1,1}} |J_1(u)|^2 du + \oint_0^{\chi'_{1,1}} |J'_1(u)|^2 du \right] \quad (10)$$

were Z_0 is the characteristic impedance in the free space, a_0 is the radius of the waveguide. J_1 and J'_1 are the first order Bessel function and its respective derivative. $\chi'_{1,1}$ is the first non-vanishing root of the equation:

$$J'_1(x) = 0$$

and

$$k_0 = \frac{\omega}{c}; \quad k_{t_{1,1}} = \frac{\chi'_{1,1}}{a_0}; \quad k_{z_{1,1}} = \sqrt{k_0^2 - k_{t_{1,1}}^2}$$

The total attenuation along the foil of length l_g is described by the formula:

$$A_{cyl} = \int_0^{l_g} \alpha_{cyl} dz = \alpha_{cyl} l_g \quad (11)$$

where l_g is the length of the waveguide.
To check our analytical tool, we evaluate the agreement between a numerical code and our formula for various coating thickness with a NEG conductivity value of $\sigma_{coat} = 3.5 \ 10^5 \ S/m$, which is one of the estimated values in the already quoted paper [12].
We evaluate the relative attenuation (see Eq.9) for the cylindrical waveguide as:

$$RA_{cyl} \triangleq A_{cyl}^{cu} - A_{cyl}^{coat} \quad (12)$$

The comparison between our analytical evaluation (Eq. 12) and CST Frequency Domain simulation is shown in Fig.9.
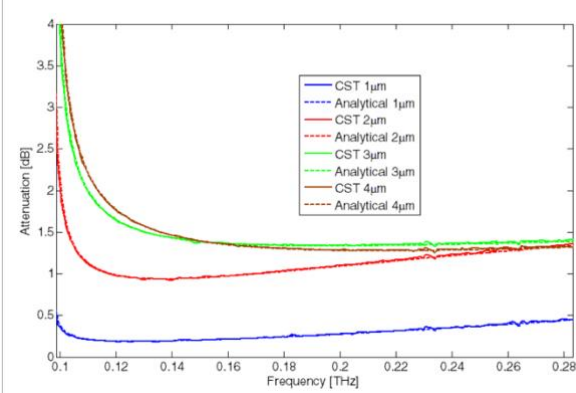

Figure 9: Relative attenuation of the first mode on the foil for different coating thickness with $\sigma_{coat} = 3.5 \ 10^5 \ S/m$. Comparison between analytical formulas and CST Frequency Domain simulations.

The excellent agreement makes it hard to detect any discrepancies between CST simulations and our theory.

Estimation on the foil in the pyramidal transition

The attenuation on the foil interposed on the center of the pyramidal transition is due to the sum of two degenerate modes. The foil forces the propagation of the first two modes because of the boundary conditions on the metallic foil as visible in Fig. 7.
The total attenuation per unit length is:

$$\alpha_{pyr}(z) = \sqrt{2} \frac{Re(Z_S) k_{z_{sum}}(z)}{a(z) Z_0 k_0} \left[1 + \frac{2 k_{t_{sum}}^2(z)}{k_{z_{sum}}^2(z)} \right] \quad (13)$$

The total attenuation on the foil in the two transitions is not anymore a constant, because the side is changing along the waveguide, this means that the attenuation of two modes on the pyramidal walls is given by the resolution of the integral:

$$A_{pyr} = 2 \int_0^{l_t} \alpha_{pyr}(z) dz =$$

$$\sqrt{2} \frac{Re(Z_S)}{Z_0} \left[-\frac{1}{2d} log \left[\frac{\sqrt{1 - \left(\frac{\pi}{k_0 B}\right)^2} - 1}{\sqrt{1 - \left(\frac{\pi}{k_0 B}\right)^2} + 1} \frac{\sqrt{1 - \left(\frac{\pi}{k_0 a}\right)^2} + 1}{\sqrt{1 - \left(\frac{\pi}{k_0 a}\right)^2} - 1} \right] + \right.$$

$$\left. \frac{2}{d} \left[\sqrt{1 - \left(\frac{\pi}{k_0 B}\right)^2} - \sqrt{1 - \left(\frac{\pi}{k_0 a}\right)^2} \right] \right] \quad (14)$$

Where

$$a(z) = b + zd = b + \frac{z(B - b)}{l_t}$$

is formula of the side of the waveguide that changes along the transition, l_t is the longitudinal length of the transition and B is the side of the entrance of the pyramidal horn transition and

$$k_{t_{sum}}(z) = \frac{\pi}{a(z)}; \quad k_{z_{sum}}(z) = \sqrt{k_0^2 - k_{t_{sum}}^2}$$

We evaluate the relative attenuation (see Eq.9) for the Pyramidal transition as:

$$RA_{pyr} \triangleq A_{pyr}^{cu} - A_{pyr}^{coat} \quad (15)$$

The comparison between this analytical evaluation and the CST Frequency domain solver is in Fig. 10 for $\sigma_{coat} = 3.5 \ 10^5 \ S/m$.
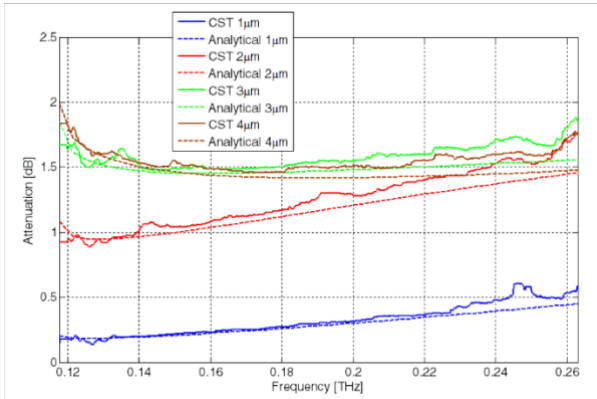
Figure 10: Attenuation of two modes on foil in pyramidal transition for different coating thickness with $\sigma_{coat} = 3.5 \ 10^5 \ S/m$. Comparison between analytical formulas and CST Frequency Domain simulations.

THE MEASUREMENT CAMPAIGN

Before starting the measurements with the coated slabs, the symmetry of the waveguide has been tested without any slab. The time domain signal passing through the waveguide has been compared with the one passing in the same waveguide rotated by 90 degrees, keeping constant the direction of the electric field. The two signals in Fig. 11 are almost superimposed. This verifies that the waveguide is top-bottom and left-right symmetric.
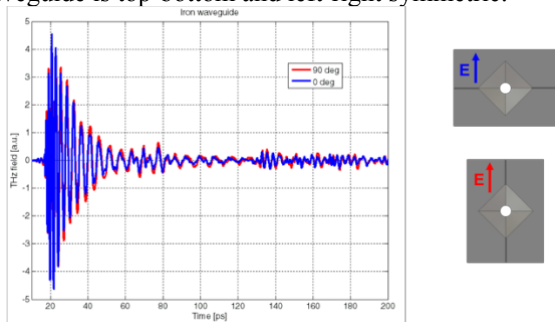

Figure 11: Test of the top-bottom left-right symmetries. The waveguide is 90 degree rotated (red) with respect to the normal use (blue). The polarization of the incident wave is taken constant.

After this check, the measurements have been performed on a waveguide with copper slab placed in the center as reference and then two different NEG coated copper slabs with 3.9 μm and 3.7 μm of coating thickness.
The spectrum of the first set of measurements in the frequency range of our interest is shown in Fig. 12
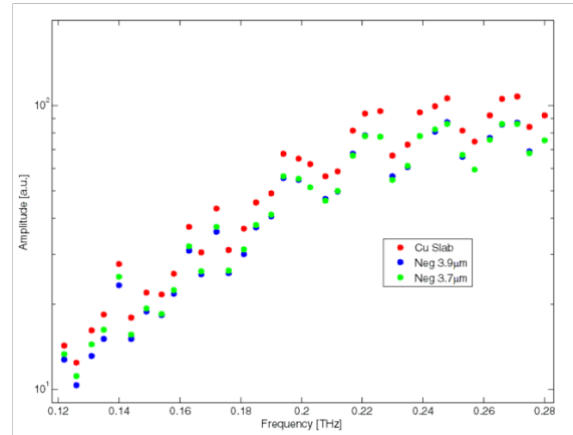

Figure 12: Fourier transform of three different measurements. Waveguide with copper slab (red), waveguide with NEG coated slab of 3.9 μm (blue) and waveguide with NEG coated slab of 3.7 μm (green)

The pattern shows the attenuation due to the presence of the coating on the two different slabs with the respect to the copper one. After preliminary settings of the lens and the maximization and symmetrization of the signal in the waveguide, we carried out 5 repeated measurements to evaluate the attenuation.

Furthermore, at the lowest frequencies, the noise distorts the signal and can introduce artificial phase discontinuities, making the phase unwrapping difficult and producing artifacts in the data spectrum [21]. For this reason, we discarded the data below 160 GHz, and in the following, all results are presented in the range 160 - 283 GHz.

The Fig.13 shows the conductivity evaluation for the NEG coating of 3.9 μm. The signal is compared with theoretical curves with different conductivity of the coating. The best fit, evaluated with the least square method, estimates $\sigma_{coat} = 7.9 \ 10^5 \ S/m$ with an error of 7%.
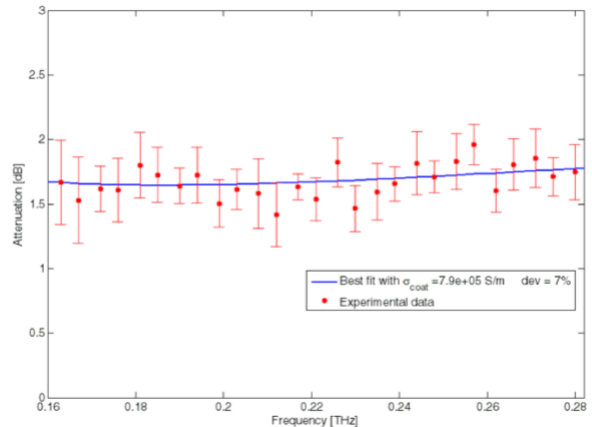

Figure 13: Attenuation on the NEG coated slab of 3.9 μm: averaged experimental data (red dots) and best fit curve (blue).

The measurements have been also performed with a different copper slab with a NEG coating of 3.7 μm.

In Fig.14 σ_{coat} is estimated to be 8.2 10^5 S/m. In this case the error is in the order of 10%, this high value could be caused by a peel-off on the extremal part of the foil.
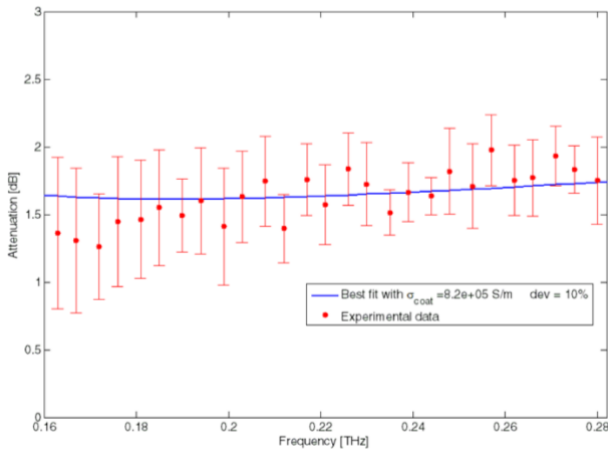

Figure 14: Attenuation on the NEG coated slab of 3.7 μm: averaged experimental data (red dots) and best fit curve (blue).

CONCLUSIONS

The comparison between the analytical evaluation and the numerical solution shows a good agreement. The developed analytical method is reliable. The advantages of the setup with the central coated slab are both intrinsic simplification of the manipulation of all the setup and the possibility to have a uniform deposition on the flat slab. The evaluated coating of the NEG sample for the two different slab goes from 7.9 10^5 S/m to 8.2 10^5 S/m with a maximum error in the estimation of the 10%.

The surface impedance is estimated in figures 15 and 16. That value is derived both from the performed measurements and from the best fit value of conductivity.
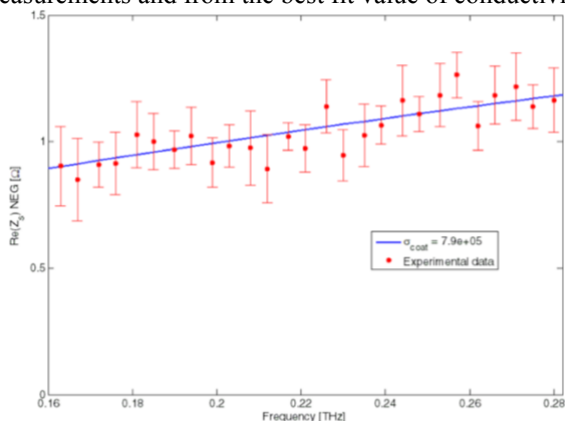

Figure 15: Surface impedance estimation of the 3.9 μm NEG coated slab: from averaged experimental data (red dots) and from best fit curve conductivity (blue).
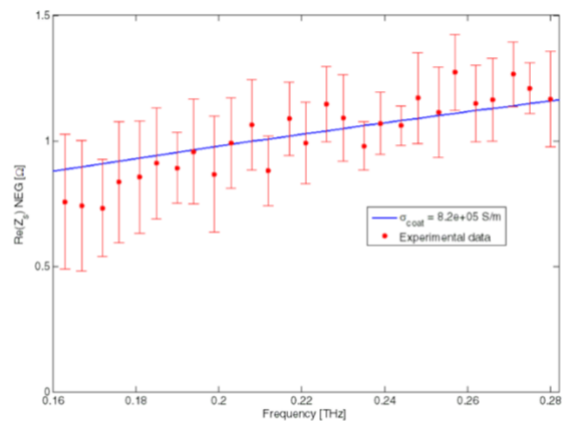

Figure 16: Surface impedance estimation of the 3.7 μm NEG coated slab: from averaged experimental data (red dots) and from best fit curve conductivity (blue).

After the Ecloud'18 workshop where this paper has been presented, a more complete version of the article and following studies on the methodology have been published in [22, 23].

ACKNOWLEDGEMENTS

REFERENCES

[1] C. Yin Vallgren et al., Amorphous carbon coatings for the mitigation of electron cloud in the CERN Super Proton Synchrotron. Phys. Rev. ST Accel. Beams 14, 071001 (2011).

[2] C. Benvenuti, P. Chiggiato, F. Cicoira, and V. Ruzinov, Decreasing surface outgassing by thin film getter coatings Vacuum, 50, 57 (1998).

[3] M.A. Furman, Electron Cloud Effects in Accelerators, arXiv:1310.1706, Oct 2013, https://cds.cern.ch/record/1606733.

[4] G. Rumolo, F. Ruggiero and F. Zimmermann, Simulation of the electron-cloud build up and its consequences on heat load, beam stability, and diagnostics,Phys. Rev. ST Accel. Beams, 4, 012801, Jan 2001, 10.1103/Phys-RevSTAB.4.012801.

[5] R. Cimino, L.A. Gonzalez, R. Larciprete A. Di Gaspare, G. Iadarola and G. Rumolo, Detailed investigation of the low energy secondary electron yield of technical Cu and its relevance for the LHC, Phys. Rev. Spec. Top. Accel. Beams, 2015, https://cds.cern.ch/record/2136495

[6] M. Taborelli, P. Chiggiato, P.C. Pinto, P. Cruikshank, Nine years of carbon coating development for the SPS upgrade: achievements and heritage. CDS: CERN-ACC-2016-0010.

[7] M. A. Palmer, J. P. Alexander, M. G. Billing , J. R. Calvey & et al. in Proc. 1st Int. Particle Accelerator Conf., 23-28 May 2010, Kyoto, Japan (2010), 12511255.

[8] C. Benvenuti,R. Calder and O. Grobner, Vacuum for particle accelerators and storage rings, Vacuum, 37(6):699 - 707, 1987.

[9] C. Benvenuti, P. Chiggiato, F. Cicoira, and V. Ruzinov, Decreasing surface outgassing by thin film getter coatings, Vacuum 50, 57 (1998), electronic Properties of Metal/Non-Metal Microsystems.

[10] M. Migliorati, E. Belli and M. Zobov, Impact of the resistive wall impedance on beam dynamics in the Future Circular e+e- Collider, Apr 2018, American Physical Society, 10.1103/PhysRevAccelBeams.21.041001, https://link.aps.org/doi/10.1103/PhysRevAccelBeams.21.041001

[11] C. Benvenuti, P. Chiggiato, P. C. Pinto, A. Prodromides, and V. Ruzinov, Influence of the substrate coating temperature on the vacuum properties of TiZrV nonevaporable getter films, Vacuum 71, 307 (2003).

[12] E. Koukovini-Platia, G. Rumolo and C. Zannini Electromagnetic characterization of nonevaporable getter properties between 220330 and 500750 GHz for the Compact Linear Collider damping rings Phys. Rev. ST Accel. Beams 20, 011002 (2017)

[13] E. Koukovini Platia, L. Rivkin and G. Rumolo, High Frequency effects of Impedances and Coatings in the CLIC Damping Rings, 2015, https://cds.cern.ch/record/2056739

[14] M. Aicheler, P. Burrows, M. Draper, T. Garvey, P. Lebrun, K. Peach, N. Phinney, H. Schmickler, D. Schulte and N. Toge, A Multi-TeV Linear Collider Based on CLIC Technology: CLIC Conceptual Design Report, Geneva, CERN-2012-007, 2012, https://cds.cern.ch/record/1500095

[15] CST Microwave Studio - Getting started (2003)

[16] J. F. Johansson and N. D. Whyborn, The diagonal horn as a sub-millimeter wave antenna, May 1992, IEEE Transactions on Microwave Theory and Techniques

[17] S. Silver , Microwave antenna theory and design, IET, Stevenage, Electromagnetic waves, 1983, https://cds.cern.ch/record/212162

[18] C. S. Lee, and S. W. Lee, and S. L. Chuang, Plot of Modal Field Distribution in Rectangular and Circular Waveguides, Microwave Theory and Techniques, IEEE Transactions on Microwave Theory Techniques, Mar 1985, 10.1109/TMTT.1985.1132998.

[19] N. Marcuvitz, Waveguide Handbook, 1986

[20] G. Franceschetti, Electromagnetics: Theory, Techniques, and Engineering Paradigms, 1997, Springer US

[21] W. Withayachumnankul and M. Naftaly, Journal of Infrared, Millimeter, and Terahertz Waves 35, 610 (2014).

[22] Passarelli, A.; Bartosik, H.; Rumolo, G.; Vaccaro, V.G.; Masullo, M.R.; Koral, C.; Papari, G.P.; Andreone, A.; Boine-Frankenheim, O. Novel measurement technique for the electromagnetic characterization of coating materials in the sub-THz frequency range. Phys. Rev. Accel. Beams 2018, 21, 103101, doi:10.1103/PhysRevAccelBeams.21.103101.

[23] Passarelli, A.; Koral, C.; Masullo, M.R.; Vollenberg, W.; Lain Amador, L.; Andreone, A. Sub-THz Waveguide Spectroscopy of Coating Materials for Particle Accelerators. Condens. Matter 2020, 5, 9.

90